Flow Turbulence Combust (2018) 101:413–432
https://doi.org/10.1007/s10494-018-9897-3

A Band-Width Filtered Forcing Based Generation of Turbulent Inflow Data for Direct Numerical or Large Eddy Simulations and its Application to Primary Breakup of Liquid Jets

Sebastian Ketterl[1] · **Markus Klein**[1]

Received: 12 October 2017 / Accepted: 20 February 2018 / Published online: 8 March 2018

Abstract Direct Numerical Simulation (DNS) and Large Eddy Simulation (LES) of spatially inhomogeneous flows strongly depend on turbulent inflow boundary conditions. Realistic coherent structures need to be prescribed to avoid the immediate damping of random velocity fluctuations. A new turbulent inflow data generation method based on an auxiliary simulation of forced turbulence in a box is presented. The new methodology combines the flexibility of the synthetic turbulence generation with the accuracy of precursor simulation methods. In contrast to most auxiliary simulations, the new approach provides full control over the turbulence properties and computational costs remain reasonable. The lack of physical information and artificiality attested with pseudo-turbulence methods is overcome since the inflow data stems from a solution of the Navier-Stokes equations. The generated velocity fluctuations are by construction divergence-free and exhibit the non-Gaussian characteristics of turbulence. The generated inflow data is applied to the simulation of multiphase primary breakup.

Keywords Turbulent inflow · Band-width filtered turbulence forcing · Large eddy simulation · Direct numerical simulation

1 Introduction

As a result of continuously increasing computational resources and efficient algorithms transient, turbulence resolving flow simulations become more and more common not only in academia but also for industrial applications. However, there is a strong dependency of eddy-resolving simulations for turbulent flows on the employed inflow conditions [1]. From

✉ Sebastian Ketterl
sebastian.ketterl@unibw.de

[1] Department of Aerospace Engineering, Universität der Bundeswehr München, Werner-Heisenberg-Weg 39, 85577, Neubiberg, Germany

a mathematical point of view all solutions of the Navier-Stokes equations depend on the initial and boundary conditions. However, it has been pointed out [2] that this sensitivity is less pronounced in the case of Reynolds averaged Navier-Stokes (RANS) solutions compared to Large Eddy Simulation (LES): Whereas prescribing mean profiles for first and second order statistics is sufficient in the case of RANS, hybrid RANS/LES methods, LES or Direct Numerical Simulations (DNS) require inlet data that feature realistic coherent structures.

Without any claim of completeness we provide in the following a short discussion on methods for generating turbulent inlet data. A complete review of inlet boundary conditions for unsteady flow simulations is far beyond the scope of this paper. Instead we refer to the overview given in [3, 4] as well as the literature reviews and references provided within all the articles that will be discussed in the following.

Auxiliary or precursor simulation methods (e.g. [5]) often make use of cyclic domains or alternatively a rescaling procedure [6]. They are inherently more accurate, but rescaling arguments cannot be applied to arbitrary flows. Furthermore, they may introduce artificial periodicity into the time series and there is an increased cost of simulation. If the required inlet velocity profile does not represent a fully developed flow or a flow in equilibrium that could be rescaled, it may be impossible to modify them in such a way that the required turbulence state is obtained [3, 7].

Several early methods to synthetise pseudo-turbulent inflow data are based on the knowledge or an assumption of the energy content of individual wave numbers in Fourier space [8–11]. These methods were applied with success to academic flow problems, but they have several drawbacks which make them less suitable for more applied problems [7, 12].

From an engineering perspective at least the integral length and time scales of the inflow data should be correct. Examples of such methods are the diffusion based approach [13], the synthetic eddy method [12] or the digital filter based inflow generation [7]. It is worth mentioning that the latter has been extended to recover prescribed autocorrelation functions [2] instead of the length scale only. Further, Fathalie et al. [14] demonstrated how to generate turbulent inflow and initial conditions based on multi correlated random fields with prescribed cross correlation length scales. Immer [15] included scalar turbulence and Xie and Castro [16] replaced the Gaussian filter in axial (temporal) direction with a simpler more efficient autoregressive process. Another important efficiency enhancement as well as large scale parallelisation is discussed in [17].

A particularly interesting to discuss property of inlet turbulence is often referred to as the divergence free condition. It is important to understand that this condition implicitly makes use of Taylor's frozen turbulence hypothesis which relates spatial and temporal data using a convection velocity. This is, in an instantaneous local sense, at best a valid approximation for incompressible flows where the turbulence intensity is considerably smaller than the mean flow speed [10]. Kim et al. [18] proposed a divergence-free synthetic turbulence inflow technique for incompressible flow which reduced the pressure fluctuations observed before. In the same paper these results are compared to a synthetic turbulence generation method with a correction for constant mass flux. It is found that both methods result in significant improvements on the computed pressure fluctuations. The divergence free inlet condition performs slightly better than the corrected mass flux inflow. However, the major improvement can be attributed to the mass flux correction whereas the divergence free condition has only a second order effect. These observations are consistent with the findings in the present work. It is worth noting that the divergence free condition also enforces a constant mass flux, but this is achieved at a much higher price. It is also remarked that some of the

above methods are divergence free by construction and some others are not. For example methods based on inverse Fourier transform are divergence free in an analytical sense. This does however not imply that they are divergence free when using a particular discretization scheme. Another example for synthesis of divergence free velocity fields can be found in [19].

Artificially generated turbulence has the advantage that it can be more easily adjusted to meet the desired or measured turbulence properties compared to auxiliary simulations. However, such data do not represent the solution to the Navier-Stokes equation and therefore a certain development section is required until the flow represents a realistic solution of the governing equations. It is the goal of this work to present a new methodology that combines the flexibility of the synthetic turbulence generation with accuracy of precursor simulation methods. By construction the velocity field will be divergence free.

Before presenting the new method it is worth mentioning that the use of synthetic inflow turbulence or the band-width filtered forcing inflow generation presented here is not always the best available choice and should be limited to the following applications:

- Situations where parametric studies of turbulence quantities are desirable.
- Flow configurations where standard periodic boundaries, possibly with scaling or rescaling, will not result in the desired mean velocity or turbulence profiles or two point correlations.
- Applications where precursor simulations are not possible because of exaggerated computational cost.
- Applications where boundary conditions are unknown and have to be estimated.
- Specification of inflow conditions to inlet extensions that have already been considered in the computational geometry, but at an upstream location where sensitivity of inflow specification on the main simulation is limited.

2 New Concept of Inflow Data Generation

The new concept to generate turbulent inflow data is based on an auxiliary simulation of forced turbulence in a box with full control over the turbulence properties, shown in Fig. 1. In the absence of any driving mechanism, turbulence decays and dissipates within the auxiliary simulation. In order to generate a large time series of turbulent inflow data, turbulence has to be maintained. Therefore, turbulence is continuously excited by a driving

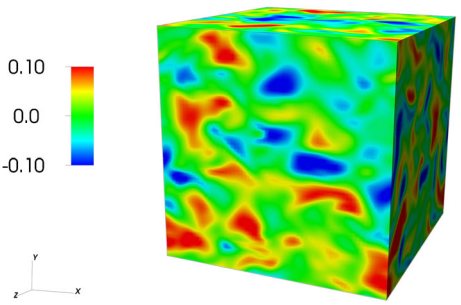

Fig. 1 Instantaneous view of a velocity component u_i of the forced box turbulence simulation

force, following the ideas of Lundgren [20], which prevents the decay of the global kinetic energy. The turbulence excitation manifests as a source term f_i in the momentum Eq. 2 of the incompressible Navier-Stokes equations

$$\frac{\partial u_i}{\partial x_i} = 0 \tag{1}$$

$$\rho\left(\frac{\partial u_i}{\partial t} + \frac{\partial u_i u_j}{\partial x_j}\right) = -\frac{\partial p}{\partial x_i} + \frac{\partial}{\partial x_j}\left(\mu\left(\frac{\partial u_i}{\partial x_j} + \frac{\partial u_j}{\partial x_i}\right)\right) + f_i \tag{2}$$

where ρ and μ denote the fluid density and viscosity, u_i and p are the velocity components and the pressure. Equation 1 enforces the incompressibility constraint.

Besides the conservation of the global turbulent kinetic energy, the uncontrolled development of the integral length scale associated with turbulence forcing [21], needs to be prevented in order to guarantee control over the integral length scale. The new procedure is based on band-width filtered turbulence forcing [22]. The linear turbulence excitation term takes the following form

$$f_i = A_i \overline{u'_i}^{HP}. \tag{3}$$

The source term consists of a control parameter A_i and is chosen proportional to a high pass filtered velocity fluctuation $\overline{u'_i}^{HP}$. The parameter A_i can in principle depend on the coordinate direction i considered and as well on space and time. Details will be discussed in Sections 2.1 and 2.2 respectively.

The driving force f_i plays the essential role in the new procedure: it controls the turbulence in the box simulation. On the one hand, the driving force excites turbulence and prevents the turbulence decay by dissipation. This ensures a certain turbulence intensity of velocity fluctuations of the inflow data and allows the generation of a large time series of inflow data. On the other hand, a driving force proportional to a high pass filtered velocity fluctuation allows control of the integral length scale of the velocity fluctuations. The generation of the turbulent boundary condition needs two input parameters: the desired turbulence intensity $\sqrt{\langle u'_i u'_i \rangle_t}$ and the desired integral length scale l of the inflow data, two parameters of the flow one often has an intuitive feeling from the engineering point of view. The procedure is as follows:

1. Generate turbulent velocity fluctuation u'_i of the desired fluctuation level $\sqrt{\langle u'_i u'_i \rangle_t}$ and desired integral length scale l in the auxiliary simulation of forced box turbulence.
2. Choose a fixed plane arbitrarily located in the box. For this plane extract and store a time sequence of data from the auxiliary simulation.
3. Superpose the extracted velocity fluctuation u'_i to the desired mean velocity profile $u_{i,mean}$.
4. Apply the planes as turbulent inflow data / turbulent boundary condition to the application of interest.

The inflow data is by construction divergence-free. The generated velocity fluctuations stem from a solution of the Navier-Stokes equations and hence constitute a solenoidal vector field

$$\frac{\partial u'_i}{\partial x_i} = 0. \tag{4}$$

If the velocity fluctuations are superposed on the mean velocity profile $u_{i,bc} = u_{i,mean} + u_i'$, the resulting velocity profile $u_{i,bc}$ remains solenoidal if the mean velocity profile itself

$$\frac{\partial u_{i,mean}}{\partial x_i} = 0. \tag{5}$$

is divergence-free. For an injection nozzle with x and u_{mean} being the axial direction and the axial injection velocity, the divergence-free condition of the mean velocity reduces to $\partial u_{mean}/\partial x = 0$ if the lateral and homogeneous velocities are zero $v_{mean} = w_{mean} = 0$.

The domain size of the precursor turbulent box simulation is chosen according to the dimensions of turbulent inflow region in the main simulation: If the domain for the application of interest contains a turbulent inlet region corresponding to the outlet plane of a hypothetical injection nozzle with diameter D, the dimensions of the box simulation are chosen to be $D \times D \times D$. It is recommended to use the same resolution in the precursor simulation as in the inflow plane of the main simulations. In order to guarantee a fully developed turbulent flow field in the auxiliary box simulation, the viscosity is adjusted based on the prescribed fluctuations level, the length scale and the grid resolution. With the applied number of grid points N in each direction, the maximum resolvable turbulence Reynolds number Re_L and Taylor microscale Reynolds number Re_λ within the auxiliary simulation are estimated by

$$Re_L \sim \left(\frac{N}{1.6}\right)^{4/3} \qquad Re_\lambda \sim \left(\frac{N}{0.4}\right)^{2/3} \tag{6}$$

according to the theory for DNS of homogeneous turbulence [23]. The turbulence Reynolds number Re_L and Taylor microscale Reynolds number Re_λ are defined as

$$Re_L = \frac{k^{1/2}\, L}{\nu} = \frac{k^2}{\nu\, \epsilon} \qquad Re_\lambda = \frac{u_i'\, \lambda_g}{\nu} \tag{7}$$

where L is the length scale characterizing the large eddies, λ_g denotes the transversal Taylor microscale and k is the turbulent kinetic energy. With the prescribed turbulence intensity $\sqrt{\langle u_i' u_i' \rangle_t}$, the targeted turbulent kinetic energy is calculated by

$$k = \frac{1}{2} \langle u_i' u_i' \rangle_t. \tag{8}$$

From the targeted turbulent kinetic energy and the length scale, the dissipation rate ϵ is estimated by

$$\epsilon = \frac{(k)^{3/2}}{L} \tag{9}$$

The ratio of the integral length scale and the length scale of the largest turbulent eddies l/L is estimated from chapter 6 of Popes's book [23]. The ratio is a function of the Reynolds number and converges to an asymptotic value of 0.43 for large Reynolds numbers. For moderate Reynolds numbers, e.g. $Re_\lambda = 22$ for $N = 64$, the ratio can be estimated as 0.6. The dissipation rate is then approximated by

$$\epsilon = \frac{(k)^{3/2}}{l/0.6}. \tag{10}$$

Hence, the smallest viscosity which can be applied to the auxiliary simulation for a prescribed turbulence intensity and a fixed grid size N is

$$\nu = \frac{k^2}{\epsilon\, Re_L}. \tag{11}$$

This lower viscosity limit ensures a fully resolved turbulent flow field down to the smallest scales of turbulent motion. The upper limit of the viscosity is defined according to [24] who observed that the skewness factor of the turbulent field, see Section 2.3, collapses for small Re_{λ_g}. In order to guarantee sufficient nonlinear interaction in turbulence, the minimum Taylor microscale Reynolds number is set to $Re_{\lambda_g,min} = 10$ following [25]. Calculating the Taylor microscale based on [23] by

$$\lambda_g = l\sqrt{10}\, Re_L^{-1/2}, \tag{12}$$

the highest applicable viscosity is given by

$$\nu = \frac{u_i' \lambda}{Re_{\lambda_g,min}}. \tag{13}$$

The lower limit of the Taylor microscale number also influences the general applicability of the turbulent boundary condition generation. To ensure a sufficiently high Taylor microscale number, the lower limit of grid resolution across the inflow nozzle is 12 control volumes $\left(N \sim Re_\lambda^{3/2}\right)$.

The initial turbulent velocity field in the auxiliary box simulation is generated by an extension of Klein's digital filter [7] to three dimensions. The method generates an artificial velocity field of the prescribed integral length scale and turbulent intensity.

The next two sections focus on the control of the turbulence in the auxiliary box simulation. The control of the intensity by the control parameter A_i and the control of the integral length scale by the filter operation of the high pass filtered velocity fluctuation $\overline{u'}_i^{HP}$ is explained in more detail. The evaluations of the characteristics of the generated velocity fluctuations, illustrations of turbulent intensity, integral lengths etc., in the following sections are solely based on the time series of the extracted planes of inflow data.

2.1 Control of turbulence intensity

The fluctuation level of the turbulence in the box is controlled by the parameter A_i of the forcing term Eq. 3. A simple control mechanism, proposed in [22],

$$A_i = \max\left[0\ ,\ \frac{\sqrt{\langle u_i' u_i' \rangle_t} - \sqrt{\langle u_i' u_i' \rangle}}{\Delta t \cdot \sqrt{\langle u_i' u_i' \rangle_t}}\right] \tag{14}$$

regulates the forcing strength. The time step size is denoted with Δt. The target value $\sqrt{\langle u_i' u_i' \rangle_t}$ (no summation) is the prescribed specific turbulence intensity level. The targeted turbulence intensity is one of two input parameters required for the inflow data approach. The fluctuation level in Eq. 14 is a suitable spatially averaged value of the box turbulence, expressed by the brackets $\langle ... \rangle$. In case of a uniform turbulence level, the average is defined as the mean value over the three dimensional box. Figure 2 shows the fluctuation level of all velocity components. A uniform turbulence level of 2%, 5% and 10% is prescribed for all velocity components $\sqrt{\langle u'u' \rangle_t} = \sqrt{\langle v'v' \rangle_t} = \sqrt{\langle w'w' \rangle_t}$. For illustration purposes, the data is plotted over the diameter y/D of a potential injection nozzle. The fluctuations are temporally and spatially averaged in planes normal to injection nozzle height.

The desired fluctuation level for the velocity components do not need to be equal but can be prescribed individually, e.g. $\sqrt{\langle u'u' \rangle_t} \neq \sqrt{\langle v'v' \rangle_t}$. Furthermore, the turbulence intensity

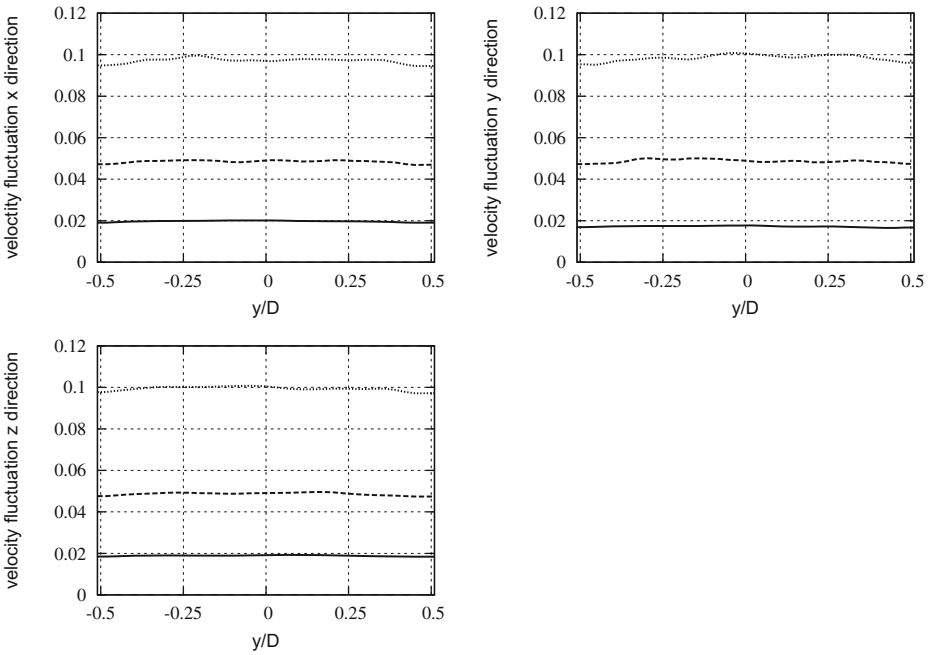

Fig. 2 Uniform turbulence intensity for axial $\sqrt{\langle u'u' \rangle}$ (top left), lateral $\sqrt{\langle v'v' \rangle}$ (top right) and homogeneous $\sqrt{\langle w'w' \rangle}$ (bottom left) velocity fluctuations at fluctuation levels 2%, 5% and 10%. Velocity fluctuations are temporally and spatially averaged

can be either uniform or defined locally, i.e. $\sqrt{\langle u_i' u_i' \rangle_t(x)}$, which allows spatially varying fluctuation levels. In this case, the spatial mean values $\langle ... \rangle$ in Eq. 14 are spatially averaged in planes normal to injection nozzle height. If e.g. channel flow turbulence characteristics are desired, spatially varying fluctuation levels are of interest. The performance of the inflow generation method is next illustrated by prescribing DNS data of a fully developed channel flow simulation at $Re_\tau = 395$ extracted from [26]. For this application the periodic boundary condition is replaced by a no-slip condition at the channel wall in order to ensure zero fluctuations at this location. Figure 3 shows the averaged velocity fluctuations $\langle u_i' u_i' \rangle(y)$ plotted over the channel height y/D. The data is temporally and spatially averaged in planes normal to the channel heigth. It can be seen that the control mechanism is also able to imitate spatially varying velocity fluctuations of a channel flow.

In our implementation the high-pass filter becomes asymmetric toward the wall and hence the filter size is implicitly reduced since no filtering across the wall is carried out. The strong anisotropy of the near wall length scales is not considered. This would be possible by prescribing local, strong anisotropic filter functions similar to the work reported in [2] but is not pursued further in this work.

Prescribing the diagonal components of the Reynolds stresses has not been considered so far. However, this could be achieved as follows: Forcing for example the v-velocity component by a combination of u and v fluctuations, similar to the transformation used in Klein et al. [7], will introduce a cross correlation. A detailed investigation in this regard is left for future work.

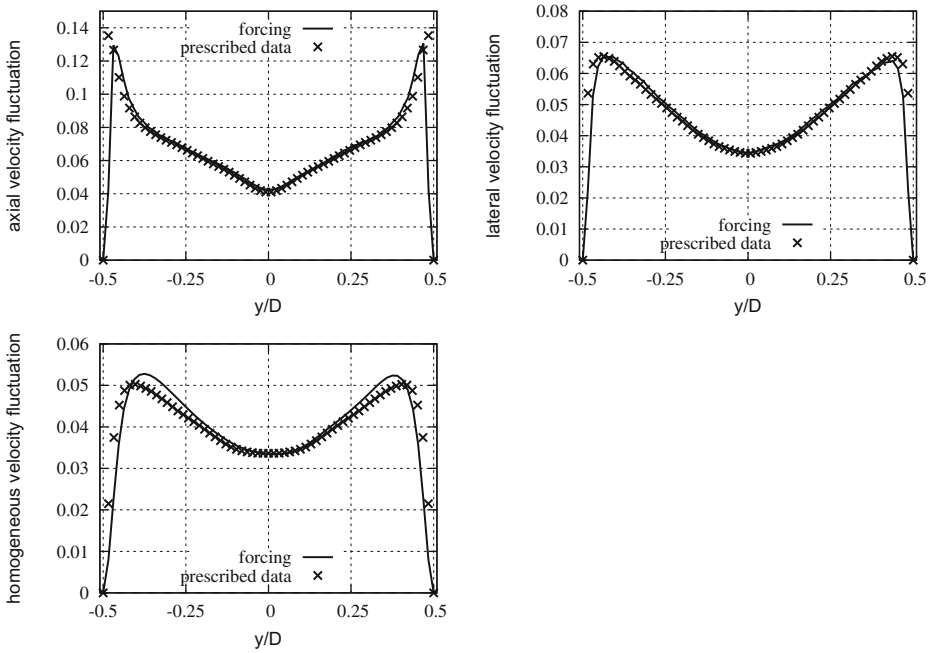

Fig. 3 Spatially varying turbulence intensity obtained by turbulence forcing in the box simulation imitating a channel flow at $Re_\tau = 395$. Shown are the axial $\sqrt{\langle u'u' \rangle}$ (top left), lateral $\sqrt{\langle v'v' \rangle}$ (top right) and homogeneous $\sqrt{\langle w'w' \rangle}$ (bottom left) velocity fluctuations plotted against the prescribed channel flow characteristics taken from Mansour et al. [26]. Velocity fluctuations are temporally and spatially averaged

2.2 Control of integral length scale

The control of the integral length scale of the turbulence in the box is achieved by the proportionality of the forcing term to suitably filtered velocity fluctuation $\overline{u'}_i^{HP}$ [22]. It is important to note that the mean velocity in the precursor simulation is zero. Hence, the fluctuating velocity components are used to underline that the precursor simulation generates the velocity fluctuations. The high pass filtered velocity fluctuation is obtained by applying a conventional LES convolution filter G

$$\bar{u}_i'(x) = G * u_i'(x) \tag{15}$$

to the velocity fluctuation field and subtracting the low pass filtered velocity fluctuation $\bar{u}_i(x)$ from the unfiltered velocity fluctuation

$$\overline{u'}_i^{HP} = u_i' - \overline{u'}_i. \tag{16}$$

The filter operation is carried out every time step. The Top Hat filter kernel G is a convolution of three one-dimensional filter functions

$$G(x_i) = \begin{cases} \frac{1}{L_f} & \text{if } |x_i| \leq L_f/2 \\ 0 & \text{otherwise} \end{cases} \tag{17}$$

where L_f is the filter length scale. It should be noted that the forcing method is not restricted to a top hat filter and alternatives, e.g. a Gaussian kernel, are possible. Most forcing methods are realized in spectral space e.g. [27] where energy is injected into a narrow band of

wave numbers. Turbulence forcing in physical space was proposed by Lundgren [20]. This "linear forcing" with a driving force proportional to the velocity u_i injects energy over all scales of turbulent motion. Lungren's forcing maintains the global turbulent kinetic energy spatially and temporally. The integral length scale typically converges to a constant fraction of the domain size independent of the Reynolds number and the initial conditions [21]. In order to prevent the uncontrolled growth of the integral length scale, the band-width filtered forcing shifts the injection of energy toward smaller scales of turbulence. The band-with filtered forcing circumvents the inflexibility of linear turbulence forcing and allows for variable integral length scales of the generated inflow data. The integral length scale of turbulent structures is not any longer a function of domain size but solely dependent on the filter size L_f of the convolution filter Eq. 17. The filter size L_f controls the integral length scale which is illustrated in Fig. 4 where the influence of the filter size to the obtained autocorrelation is shown. Clearly, the integral length scale grows with increasing filter width.

In order to exactly meet the prescribed integral length scale l a control mechanism regulates the filter size L_f. In analogy to the forcing parameter A_i, the control mechanism for the filter size reads

$$L_f = \min\left(\max\left(l\ , \frac{3}{2}l + 2l \cdot \frac{L_t - L}{L_t\,\Delta t}\right),\ \ D\right) \tag{18}$$

where L_t is the targeted and L the prevailing length scale characterizing the large eddies. D denotes the box size. A relation given in Pope [23] can be used to convert the targeted integral length scale l into L_t which in the context of our work can be approximated by $L_t = 0.6\,l$ but might be adapted according to the Taylor microscale Reynolds number. The prevailing length scale L of the flow is evaluated by the relation

$$L = \frac{k^{3/2}}{\epsilon} \qquad \text{with} \qquad \epsilon = \nu\left\langle \frac{\partial u_i}{\partial x_j}\frac{\partial u_i}{\partial x_j}\right\rangle \tag{19}$$

where ϵ denotes the dissipation rate.

When applying the turbulent boundary condition, planes of velocity fluctuations are extracted from the turbulent box simulation and prescribed as a time sequence as the inlet data for the main simulation. The temporal length scale of the inflow data is controlled by the time step size and the CFL number of the auxiliary simulation. The time step is determined by the global kinetic energy and the grid resolution (note again that the precursor

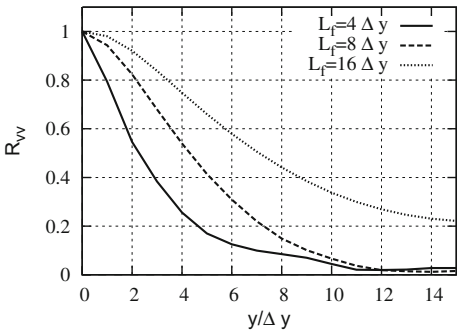

Fig. 4 Comparison of lateral autocorrelation functions depending on the filter width L_f of the spatial low pass filter G

simulation has no mean velocity). In order to meet the desired temporal integral length scale, the optimal choice of the time step is

$$\Delta t = \frac{\Delta x}{\sqrt{k}}. \tag{20}$$

If the targeted time step exceeds the CFL condition, the time step size is halved until the CFL criterion is met.

2.3 Turbulence characteristics of the inflow data

Turbulent velocity fluctuations are often regarded as random and described probabilistically. Following the classical law of large numbers, a stochastic behavior results in a normal Gaussian probability distribution. Dynamical properties of turbulence however are characterized by its non-Gaussianity [28]. This intermittency phenomenon has been verified experimentally [29, 30] and numerically [28, 31]. Small scale turbulent motion, as well as longitudinal and lateral velocity derivatives, deviate from Gaussian statistics. Intermittency is absent in larger scale properties. Non-Gaussianity of turbulence characteristics might therefore be a suitable criterion to distinguish synthetic turbulence from realistic Navier-Stokes dynamics. The generated turbulent inflow planes are analyzed with respect to turbulence statistics by examining the probability distributions of various fluctuation quantities characterizing three-dimensional turbulence.

Figure 5 displays a comparison between the forcing based turbulent inflow characteristics and a Gaussian distribution. Furthermore, inflow data characteristics generated by the digital filter based method [7], a synthetic pseudo-turbulence generation method, is added. Illustrated are velocity statistics in whole wave number space (top left) and for high wave number Fourier modes (top right). The wave number separation in physical space is realized by a high pass filter. The pdfs of the velocity fluctuation field in whole Fourier space fit well to the Gaussian for both turbulence generation procedures. Due to the increased energy contribution, large scale velocity fluctuations dominate the pdf. In contrast, high wave number velocity fluctuations deviate from Gaussian statistics, see Fig. 5 (top right). The forcing based generated inflow data reveals the nearly exponential behavior in the dissipation range bands. Figure 5 (bottom left) shows the pdf of the longitudinal velocity derivative. Forcing based inflow data deviates from the Gaussian distribution. Exponential tails arise and an asymmetric distribution is obtained. The negatively skewed distribution is an important feature of fully developed turbulence [32] and connected with stretching of vorticity [31]. The skewness and flatness of the longitudinal velocity derivative distribution in Fig. 5 (bottom left) are -0.26 and 4.2. The inflow data is generated with a Taylor microscale Reynolds number of $Re_\lambda \approx 42$. Typical skewness and flatness factors observed experimentally and numerically for increased Taylor microscale Reynolds number of $Re_\lambda \approx 90$ are around -0.4 and 4.2. The pdf of the lateral velocity derivative in Fig. 5 (bottom right) is symmetric with respect to the origin of the abscissa but forcing based inflow data also deviates from the Gaussian and approaches an exponential function.

In contrast, the pdfs of turbulence characteristics of the digital filter based inflow data are Gaussian. Non-gaussian intermittent behavior is a signature of coherence in turbulence [33]. In the presence of intermittency, a correlation among the different scales exist [28]. The pdfs underline the aspect of artificiality of synthetic pseudo turbulence generation methods

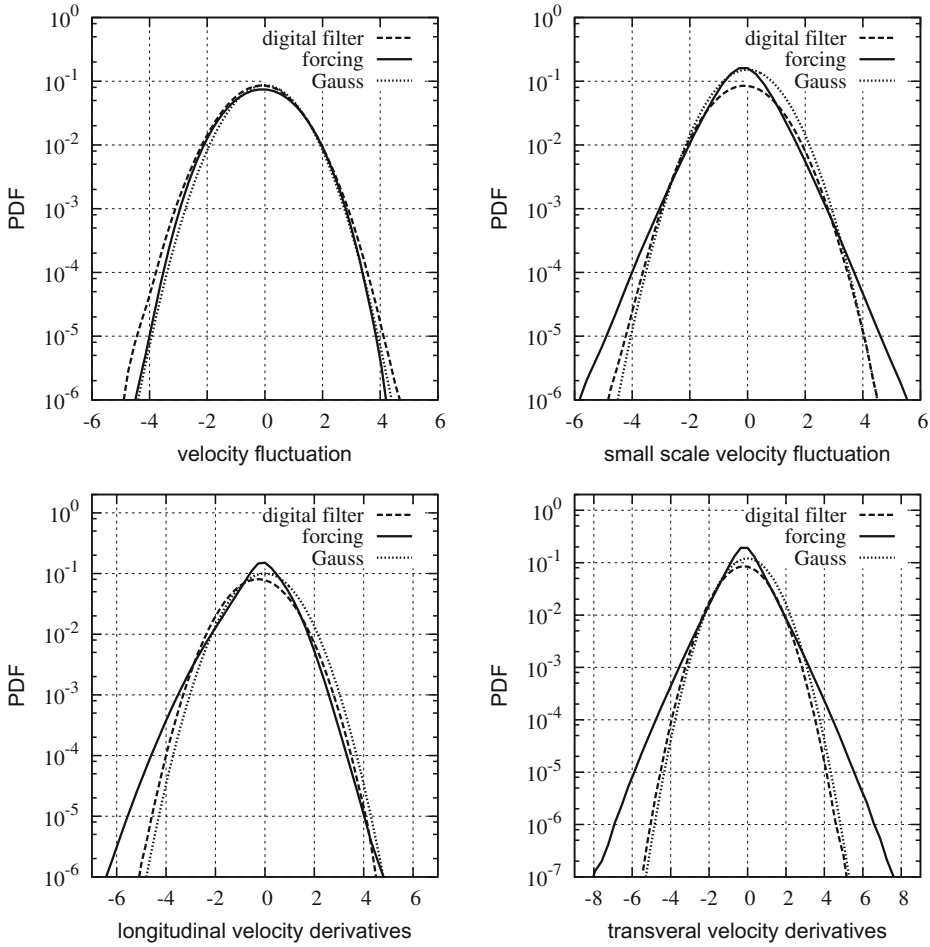

Fig. 5 Probability density functions. Displayed are the normalized velocity fluctuations $u'/\langle u'^2\rangle^{1/2}$ (top left), small scale velocity fluctuations $(u'-\overline{u'})/\langle(u'-\overline{u'})^2\rangle^{1/2}$ corresponding to high wave number modes (top right), longitudinal velocity derivatives $\partial_\alpha u'_\beta/\langle(\partial_\alpha u'_\beta)^2\rangle^{1/2}$ $(\alpha = \beta)$ (bottom left) and transveral velocity derivatives $\partial_\alpha u'_\beta/\langle(\partial_\alpha u'_\beta)^2\rangle^{1/2}$ $(\alpha \neq \beta)$ (bottom right)

and confirm the lack of physical information since fluctuating properties are not coherent as expected for fully developed turbulent structures [33]. The forcing based generated turbulence is not artificial and reveals the characteristics of turbulent motion. Realistic coherent structures are generated.

Finally, Fig. 6 shows autocorrelation functions for a uniform turbulence level and uniform length scales corresponding to isotropic turbulence. Isotropic turbulence can be fully described by its two-point correlation tensor which can be split in a longitudinal and transversal component. Batchelor [34] has shown that the two-point correlation in transversal direction correlates weaker than the longitudinal direction. This is reflected by the inflow

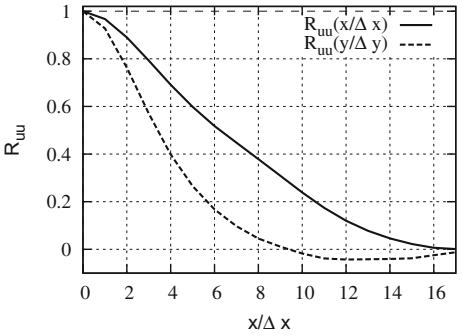

Fig. 6 Autocorrelation functions of the turbulent inflow data in longitudinal $R_{uu}(x/\Delta x)$ and transversal direction $R_{uu}(y/\Delta y)$. The transversal direction features the characteristic undershoot observed in isotropic homogeneous turbulence [34]

data in Fig. 6 which shows the longitudinal $R_{uu}(x/\Delta x)$ and transversal autocorrelation function $R_{uu}(y/\Delta y)$. Furthermore, the forced inflow data exhibits the characteristic undershoot in the transversal autocorrelation function expected for homogeneous turbulence [34]. It is worth noting that these physical features are contained in the inflow data without explicitly prescribing the desired behavior, which is in contrast to inflow generation methods which are entirely based on reproducing statistical information.

In summary, the analysis of probability distributions of the velocity fluctuations and its derivatives shows that the turbulent inflow data generated by the new forcing based method reveals more realistic dynamics compared to methods based on simply reproducing turbulence statistics.

2.4 Numerical method

The turbulent inflow data are generated with the open-source code $PARIS$-Simulator [35]. The DNS code is extended with the band-width filtered turbulence forcing described in the previous sections. The source term is added as a volume force. Numerical schemes are implemented as described in [36] where further details on numerical methods and references can be found. A projection method including a second-order predictor-corrector technique for time integration solves the Navier-Stokes Eqs. 1–2. Spatial discretization is realized by the finite-volume approach on a regular, cubic staggered grid. A second-order centered difference scheme explicitly treats the viscous term. The advection term is discretized by the third-order QUICK scheme. The QUICK scheme is only used to be consistent with the main simulation in Section 3. Since turbulence in the auxiliary simulation is fully resolved, also a simple second order central difference scheme can be used without running into stability problems. The inflow data generation is not negatively affected by the choice of the numerical advection scheme. The elliptic equation for the pressure is solved by a semicoarsening multigrid solver.

3 Application to Direct Numerical Simulation of Multiphase Primary Breakup

The turbulent inflow data is applied to the simulation of primary breakup of a planar liquid jet. Primary breakup of liquid jets is sensitive to the turbulence in the injection nozzle [7, 37, 38].

The dynamics of the two-phase liquid primary breakup are described by the one-fluid formulation of the incompressible Navier-Stokes equations including the surface tension force at the phase interface

$$\frac{\partial u_i}{\partial x_i} = 0 \tag{21}$$

$$\rho\left(\frac{\partial u_i}{\partial t} + \frac{\partial u_i u_j}{\partial x_j}\right) = -\frac{\partial p}{\partial x_i} + \frac{\partial}{\partial x_j}\left(\mu\left(\frac{\partial u_i}{\partial x_j} + \frac{\partial u_j}{\partial x_i}\right)\right) + \sigma\, n_i\, \kappa\, \delta_S. \tag{22}$$

The surface tension force consists of the interface mean curvature κ, the surface tension coefficient σ and the unit normal vector on the surface n_i. The Dirac distribution δ_S restricts the presence of capillary forces to the vicinity of the interface. The interface is tracked by an advection equation

$$\frac{\partial \alpha}{\partial t} + \frac{\partial}{\partial x_i}(\alpha\, u_i) = 0. \tag{23}$$

where the volume fraction α implicitly defines the interface between the two immiscible fluids. The volume fraction equals one in the fluid phase and zero in the gas phase respectively. Both phases are treated as one fluid with abruptly changing material properties over the phase interface. The DNS of the turbulent jet is also conducted with the $PARIS$ Simulator [35]. The interface is advected, see Eq. 23, by a volume of fluid method consisting of a Mixed Young-Centered piecewise linear interface reconstruction and a Lagrangian explicit direction split advection. A balanced Continuous-Surface-Force method computes the surface tension force. Local interface curvatures are calculated by the height-function method [39].

The primary breakup of a plane jet is shown in Fig. 7 left. The jet imitates a diesel injection at a pressure and temperature of around 5.2 MPa and 900 K and is characterized by a Reynolds number $Re = \rho_l U_0 D/\mu_l = 5000$ and a Weber number $We = \rho_l U_0^2 D/\sigma = 2000$. D denotes the jet diameter and U_0 is the mean injection velocity at the inlet. The viscosity and density ratios are set to $\mu_l/\mu_g = \rho_l/\rho_g = 40$. The computational domain is a rectangular box with dimensions $12D \times 10D \times 2D$ in axial, lateral and homogeneous jet direction. The inflow nozzle is discretized with 64 equidistant cubic control volumes. This equidistant cubic mesh resolution of $\Delta x = D/64$ is applied throughout the domain which results in $768 \times 640 \times 128$ and a total of ≈ 63 Mio. cells. Open boundaries which allow entrainment

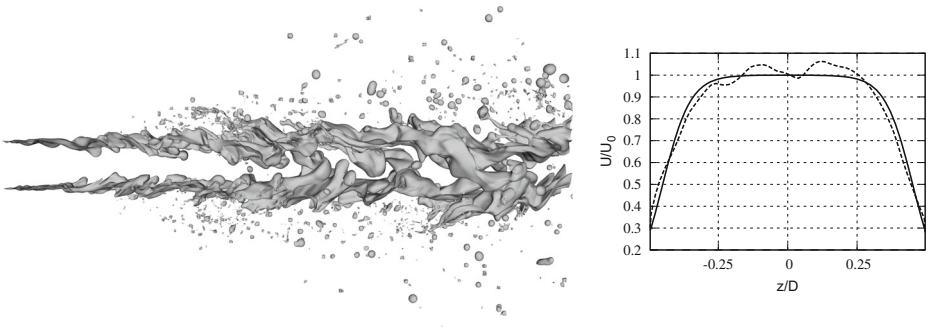

Fig. 7 Gas-liquid surface of a spatially developing plane diesel jet with the turbulent inflow data prescribed at the jet injection (left). Mean axial velocity (solid) and typical instantaneous velocity profile with superposed turbulent velocity fluctuations (dashed) (right)

characterize the lateral direction while the homogeneous direction uses the periodicity of the plane jet. A modified Neumann boundary at the outflow clips negative velocity to zero which avoids backflow and suppresses numerical instabilities. A Dirichlet boundary is set at the inlet whereas Neumann conditions are applied to all other boundaries for the volume fraction. The time step size is set constant with a CFL number $CFL = 0.2$ in the inflow nozzle which gurantees a global CFL number smaller unity. The nozzle is not included in the computational domain itself. Instead, the turbulent velocity profiles are prescribed at the inflow boundary. An axial mean velocity profile in form of a hyperbolic tangent function

$$\bar{U} = 0.5 + 0.5 \tanh\left(\frac{|y| + 0.5}{2\theta}\right) \tag{24}$$

is superposed by turbulent velocity fluctuations extracted from the auxiliary simulation of box turbulence, see Fig. 7 right which shows a typical instantaneous profile. The momentum thickness θ is $D/20$. A uniform turbulence intensity of 5%

$$\sqrt{\langle u'u' \rangle}/U_0 = \sqrt{\langle v'v' \rangle}/U_0 = \sqrt{\langle w'w' \rangle}/U_0 = 0.05 \tag{25}$$

and an integral length scale of 1/8 D which corresponds to 8 Δx is applied. The auxiliary box simulation which generates the turbulent inflow profiles is also discretized with $N = 64$ cells consistent with the number of cells across the injection nozzle. The viscosity in the auxiliary box simulation takes the value $\nu = 1.5 \cdot 10^{-4}\, m^2/s$ which results in a turbulence Reynolds number of $Re_L \approx 84$ and Taylor microscale Reynolds number of $Re_\lambda \approx 42$. The time step size to meet the desired temporal integral length scale is $\Delta t_{opt} = 0.128\, s$.

Figure 8 shows the autocorrelation functions in the three spatial directions at the inflow boundary. Integrating the autocorrelation yields an integral length scale of 8 cells (8 Δx) which corresponds to an integral length scale of 1/8 D in the inflow nozzle. The integral length scale of the generated turbulent boundary data with the new procedure is exactly reproduced in the application to the jet simulation.

The new forcing based method is compared to results obtained with the digital filter based generation of turbulent inflow data by [7]. This comparison is carried out on first and second order flow statistics. The data is averaged over 40,000 time steps corresponding to ten flow through times based on the centerline velocity. Knowing that the data is temporally uncorrelated after 200 time steps with one independent sample in homogeneous direction, $\approx$ 200 independent samples are obtained. Figure 9 displays the velocity fluctuations evaluated along the jet axis. The last two diameters of the axial length are not shown because of the upstream influence of the outflow boundary condition. At the inlet plane, turbulent fluctuations of 5% are observed reflecting the uniform turbulent intensity prescribed at the

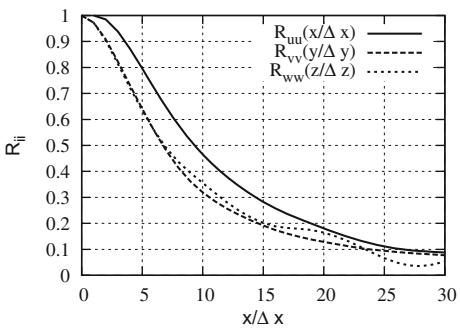

Fig. 8 Autocorrelation functions in the three spatial directions evaluated at the injection boundary at $x = 0$ of the jet simulation. The desired integral length scale of 1/8 D corresponds to 8 Δx

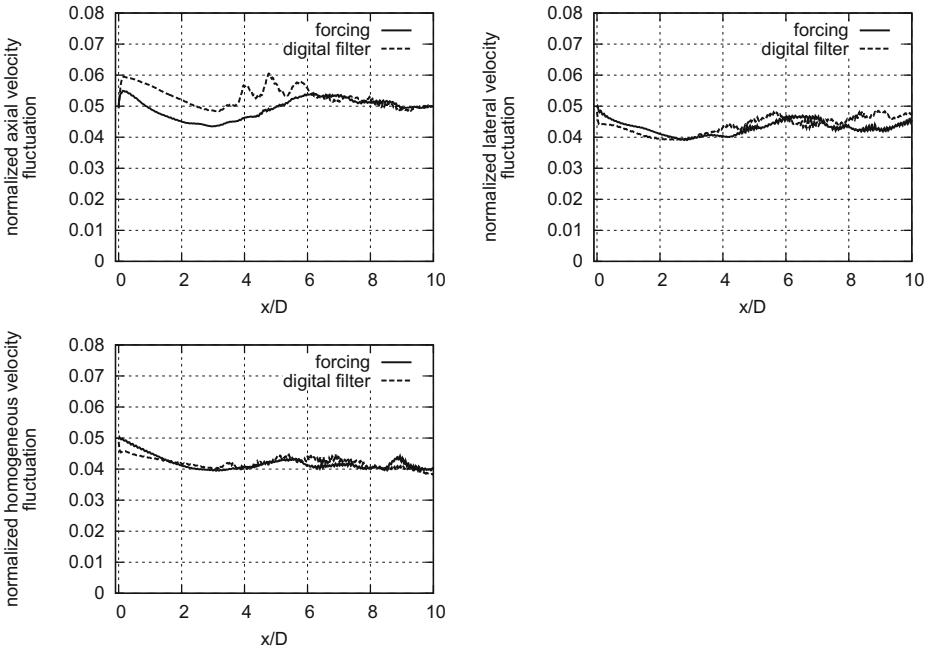

Fig. 9 Temporally averaged axial $\sqrt{\langle u'u' \rangle}/U_0$ (top left), lateral $\sqrt{\langle v'v' \rangle}/U_0$ (top right) and homogeneous $\sqrt{\langle w'w' \rangle}/U_0$ (bottom left) velocity flutuations evaluated along the jet axis

inlet. For both methods, small oscillations are visible in axial direction shortly after the inflow plane (top left). For the digital filter based approach small undershoots in the lateral (top right) and homogeneous velocity fluctuations (bottom left) can be seen before the fluctuation level remains nearly constant. In contrast, injection with the new inflow data is smoother followed by a slight decrease of the fluctuation level. In the axial velocity fluctuations, an overshoot for both methods is visible while the overshoot with the digital filter based approach is more pronounced. However, the influence of the different inflow data generation methods to second-order statistics is overall small. It can be speculated that for jet flows it is sufficient to have a reasonable initial disturbance that is able to trigger laminar

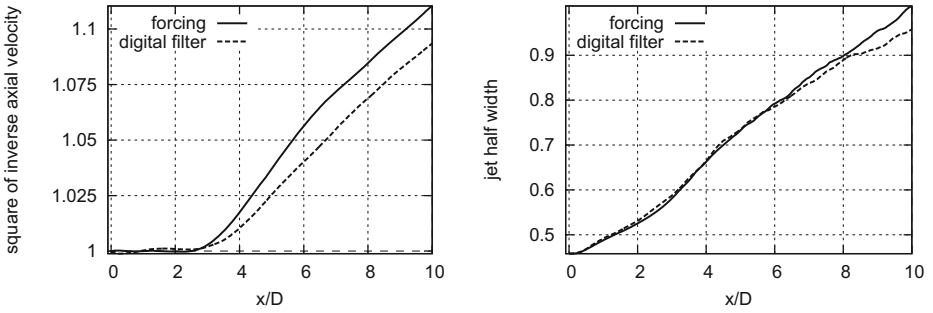

Fig. 10 Temporally averaged axial evolution of the the square of the mean injection velocity over the axial velocity $(\langle U_0 \rangle / \langle u_i \rangle)^2$ at the centerline (left) and jet half width (right)

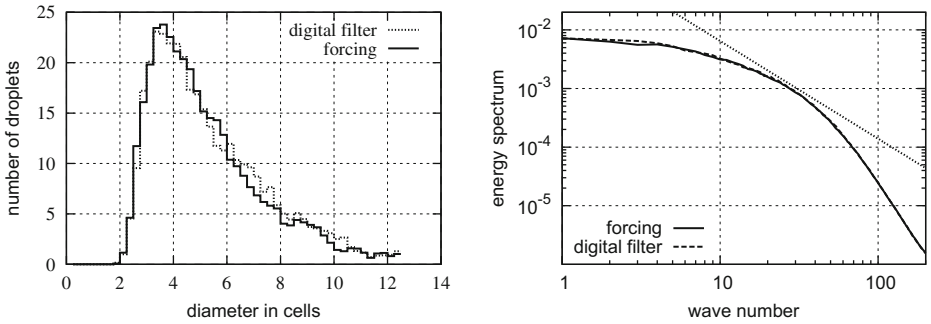

Fig. 11 Temporally averaged droplet size distribution (left) and spatial energy spectrum evaluated along the jet axis (right)

to turbulent transition. Furthermore, the mean velocity profile and corresponding boundary layer thicknesses are a relevant factor but they are independent of the inflow turbuluence.

Figure 10 shows the axial evolution of the axial velocity evaluated along the jet axis and the jet half width. The jet using the forcing based generated inflow data tends to breakup earlier. As a result, the jet spreading is slightly more pronounced.

The influence of the inflow data is further investigated by the droplet size distribution and the spatial energy spectrum of the axial velocity fluctuation, shown in Fig. 11. The droplet size distribution is averaged over 40 independant samples and the energy spectra of the axial velocity fluctuation is evaluated along the jet axis. A tendency toward smaller droplets with the forcing based inflow data is seen but the difference in the droplet size distribution between the two methods remains small. Finally, the choice of the two methods considered in this work has no influence on the energy spectrum. The energy spectrum which is shown in Fig. 11 is a spatial energy spectrum (the inhomogeneity in axial direction is implicitly contained in this spectrum) and is evaluated along the jet axis starting from $x = 2D$ to $x = 10D$. In order to apply a Fourier transformation (which is only possible for periodic signals), a Hanning window function is applied to the data.

4 Conclusions

A new method to generate turbulent inflow data has been proposed and applied to the simulation of primary breakup of a liquid jet. The method is based on an auxiliary simulation of forced turbulence in a box where turbulence forcing plays the essential role for the generation of turbulent boundary condition. It is demonstrated that band-width filtered forcing allows to generate turbulent inflow data of a prescribed integral length scale and a prescribed turbulence intensity. The turbulence level can be either uniform or spatially varying, e.g. imitating channel flow characteristics. The extracted velocity fields are by construction divergence-free since they stem from a solution of the Navier-Stokes equation. The generated inflow data reveals the non-Gaussian characteristics of turbulence while the intermittency phenomenon is absent for synthetic pseudo-turbulence generation methods. In the application to primary breakup, the influence of the new method compared to synthetic inflow data generation method is small and has to be further examined in future studies. The influence has been validated with the help of first and second order statistics as well as energy spectra and droplet size distributions. A possible explanation is that both methods are

equally well suited for triggering turbulence transition in free shear flows. The new method might be advantageous for applications where details of the small scale physics and mixing are important, e.g. combustion. Future work has to show if the improved representation of inlet flow physics in particular in terms of small scale intermittency is more beneficial for different applications. Another topic for future investigations is the appropriate consideration of anisotropic length scales in the inlet turbulence generation. This could be achieved on the one hand by using local and anisotropic filters in order to achieve the desired two point correlations similar to di Mare et al. [2] or on the other hand by inclusion of a mean velocity profile in the filtered forcing precursor simulation. Finally, the efficiency of the method depends on the details of implementation of the filtered forcing and the associated filter size. Although very efficient techniques have been developed [17] there is certainly scope for future improvements and development.

Acknowledgements Support by the German Research Foundation (Deutsche Forschungsgemeinschaft - DFG, GS: KL1456/1-1) is gratefully acknowledged. Computer resources for this project have been provided by the Gauss Center for Supercomputing/Leibniz Supercomputing Center under grant: pr48no. The authors are grateful to the developers of the *PARIS*-Simulator for providing the source code.

Funding This study was funded by Deutsche Forschungsgemeinschaft (DFG) - GS: KL1456/1-1

Compliance with Ethical Standards

Conflict of interests The authors declare that they have no conflict of interest.

Appendix

Although this paper focuses on primary atomization in the context of two phase flow liquid jets it will be instructive to repeat the analysis for a single phase plane jet. For this purpose, a comparable single phase jet has also been analyzed. An instantaneous view of the velocity magnitude of the single phase free jet is shown in Fig. 12. The domain extensions,

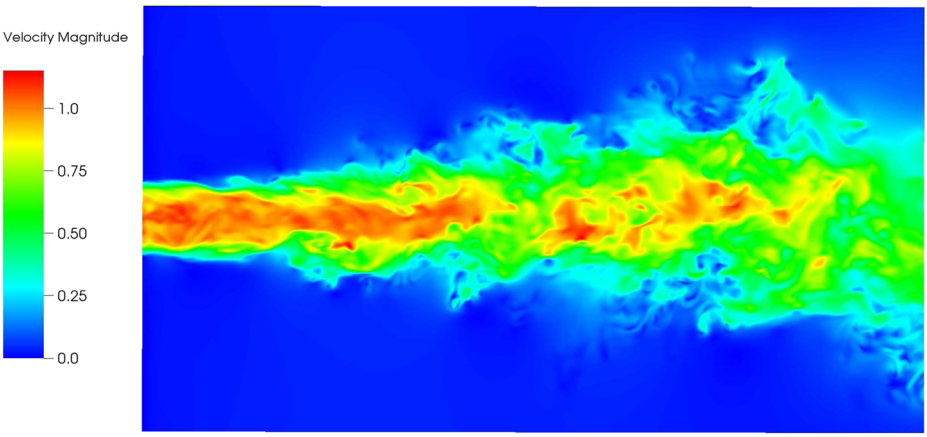

Fig. 12 Instantaneous view of the velocity magnitude of the single phase free jet

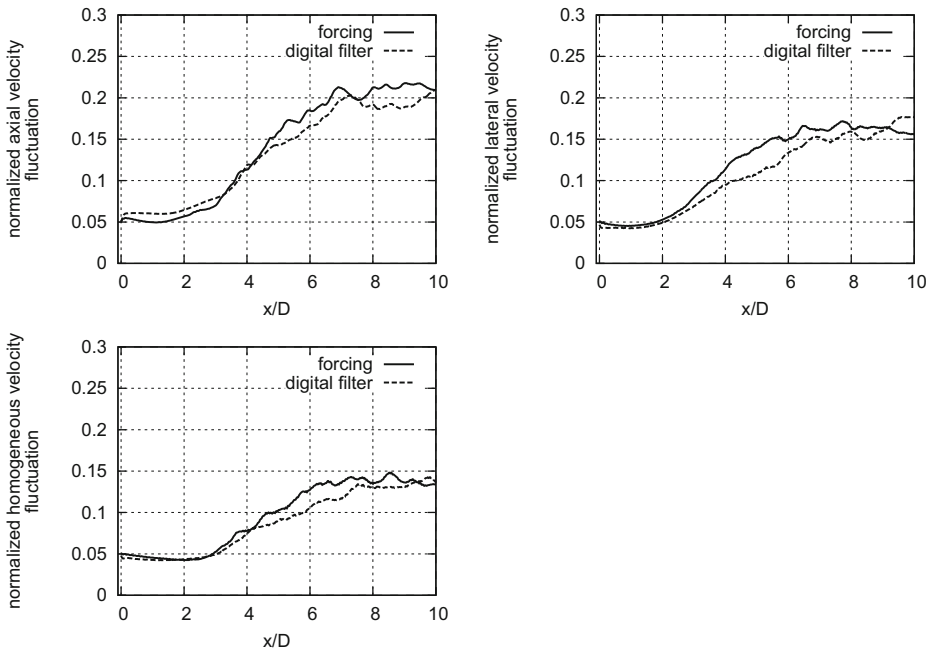

Fig. 13 Temporally averaged axial $\sqrt{\langle u'u' \rangle}/U_0$ (top left), lateral $\sqrt{\langle v'v' \rangle}/U_0$ (top right) and homogeneous $\sqrt{\langle w'w' \rangle}/U_0$ (bottom left) velocity flutuations evaluated along the jet axis of a single phase plane jet

the mesh resolution, the boundary conditions and the inflow data for both methods are identical to the two-phase jet described in Section 3. The Reynolds number is also identical $Re = \rho_l U_0 D/\mu_l = 5000$, the Weber number is not applicable for single phase flow. Figure 13 displays the velocity fluctuations evaluated along the jet axis, Fig. 14 shows the axial evolution of the axial velocity evaluated along the jet axis and the jet half width. The spatial energy spectrum of the axial velocity fluctuation is shown in Fig. 15. The droplet size distribution is not applicable for single phase flows.

The results indicate that all findings still hold true for a single phase jet. Results are qualitatively and quantitatively very similar between single and two phase flow free jets.

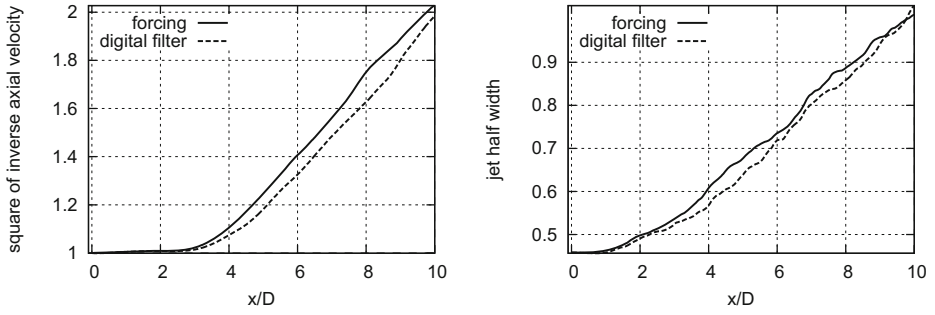

Fig. 14 Temporally averaged axial evolution of the square of the mean injection velocity over the axial velocity $(\langle U_0 \rangle / \langle u_i \rangle)^2$ at the centerline (left) and jet half width (right) of a single phase plane jet

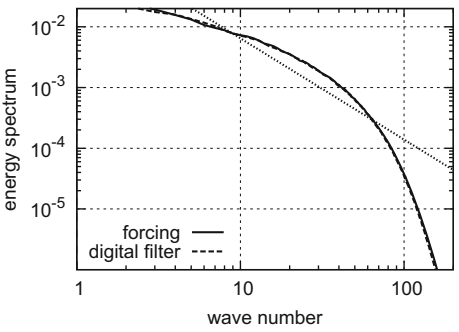

Fig. 15 Spatial energy spectrum evaluated along the jet axis of a single phase jet

References

1. Schmidt, S., Breuer, M.: Source term based synthetic turbulence inflow generator for eddy-resolving predictions of an airfoil flow including a laminar separation bubble. Comput. Fluids **146**, 1–22 (2017)
2. di Mare, L., Klein, M., Jones, W., Janicka, J.: Synthetic turbulence inflow conditions for large eddy simulation. Phys. Fluids **18**(025), 107 (2006)
3. Tabor, G., Baba-Ahmadi, M.: Inlet conditions for large eddy simulation: A review. Comput. Fluids **39**(4), 553–567 (2010)
4. Wu, X.: Inflow turbulence generation methods. Annu. Rev. Fluid Mech. **49**, 23–49 (2017)
5. Lund, T.S., Wu, X., Squires, K.D.: Generation of turbulent inflow data for spatially-developing boundary layer simulations. J. Comput. Phys. **140**(2), 233–258 (1998)
6. Tirunagari, R.R., Pettit, M.W., Kempf, A.M., Pope, S.B.: A simple approach for specifying velocity inflow boundary conditions in simulations of turbulent opposed-jet flows. Flow Turbul. Combust. **98**(1), 131–153 (2017)
7. Klein, M., Sadiki, A., Janicka, J.: A digital filter based generation of inflow data for spatially developing direct numerical or large-eddy simulations. J. Comput. Phys. **186**(2), 652–665 (2003)
8. Kondo, K., Murakami, S., Mochida, A.: Generation of velocity fluctuations for inflow boundary condition of LES. J. Wind Eng. Ind. Aerodyn. **67**, 51–64 (1997)
9. Kraichnan, R.H.: Diffusion by a random velocity field. Phys. Fluids **13**(1), 22–31 (1970)
10. Lee, S., Lele, S.K., Moin, P.: Simulation of spatially evolving turbulence and the applicability of Taylor's hypothesis in compressible flow. Phys. Fluids A: Fluid Dynamics (1989-1993) **4**(7), 1521–1530 (1992)
11. Smirnov, A., Celik, I., Shi, S.: Random flow generation technique for large eddy simulations and particle-dynamics modeling. J. Fluids Eng. **123**, 359–371 (2001)
12. Jarrin, N., Benhamadouche, S., Laurence, D., Prosser, R.: A synthetic-eddy-method for generating inflow conditions for large-eddy simulations. Int. J. Heat Fluid Flow **27**(4), 585–593 (2006)
13. Kempf, A., Klein, M., Janicka, J.: Efficient generation of initial-and inflow-conditions for transient turbulent flows in arbitrary geometries. Flow Turbul. Combust. **74**(1), 67–84 (2005)
14. Fathali, M., Klein, M., Broeckhoven, T., Lacor, C., Baelmans, M.: Generation of turbulent inflow and initial conditions based on multi correlated random fields. Int. J. Numer. Methods Fluids **57**, 93–117 (2008)
15. Immer, M.: Time-resolved measurement and simulation of local scale turbulent urban flow. Ph.D. thesis, ETH Zürich (2016)
16. Xie, Z.T., Castro, I.P.: Efficient generation of inflow conditions for large eddy simulation of street-scale flows. Flow Turbul. Combust. **81**(3), 449–470 (2008)
17. Kempf, A., Wysocki, S., Pettit, M.: An efficient, parallel low-storage implementation of Klein's turbulence generator for LES and DNS. Comput. Fluids **60**, 58–60 (2012)
18. Kim, Y., Castro, I.P., Xie, Z.T.: Divergence-free turbulence inflow conditions for large-eddy simulations with incompressible flow solvers. Comput. Fluids **84**, 56–68 (2013)
19. Kornev, N., Hassel, E.: Synthesis of homogeneous anisotropic divergence-free turbulent fields with prescribed second-order statistics by vortex dipoles. Phys. Fluids **19**(6), 068,101 (2007)
20. Lundgren, T.: Linearly forced isotropic turbulence. In: Annual Research Briefs (Center for Turbulence Research), pp. 461–473 (2003)
21. Rosales, C., Meneveau, C.: Linear forcing in numerical simulations of isotropic turbulence: Physical space implementations and convergence properties. Phys. Fluids (1994-present) **17**(9), 095,106 (2005)

22. Klein, M., Chakraborty, N., Ketterl, S.: A comparison of strategies for direct numerical simulation of turbulence chemistry interaction in generic planar turbulent premixed flames. Flow Turbul. Combust. **99**, 955–971 (2017)
23. Pope, S.B.: Turbulent flows. Cambridge University Press, Cambridge (2000)
24. Mansour, N., Wray, A.: Decay of isotropic turbulence at low Reynolds number. Phys. Fluids (1994-present) **6**(2), 808–814 (1994)
25. Trontin, P., Vincent, S., Estivalezes, J., Caltagirone, J.: Direct numerical simulation of a freely decaying turbulent interfacial flow. Int. J. Multiphase Flow **36**(11), 891–907 (2010)
26. Mansour, N., Moser, R., Kim, J.: Fully developed turbulent channel flow simulations. AGARD Advisory Report **345**, 119–121 (1998)
27. Overholt, M.R., Pope, S.B.: A deterministic forcing scheme for direct numerical simulations of turbulence. Comput. Fluids **27**(1), 11–28 (1998)
28. She, Z.S., Jackson, E., Orszag, S.A.: Scale-dependent intermittency and coherence in turbulence. J. Sci. Comput. **3**(4), 407–434 (1988)
29. Batchelor, G., Townsend, A.: The nature of turbulent motion at large wave-numbers. In: Proceedings of the Royal Society of London A: Mathematical, Physical and Engineering Sciences, vol. 199, pp. 238–255. The Royal Society (1949)
30. Monin, A.S., Yaglom, A.M.: Statistical fluid mechanics, volume II: Mechanics of turbulence, vol. 2. Courier Corporation, North Chelmsford (2013)
31. Yamamoto, K., Kambe, T.: Gaussian and near-exponential probability distributions of turbulence obtained from a numerical simulation. Fluid Dyn. Res. **8**(1-4), 65–72 (1991)
32. Smith, L., Reynolds, W.: On the Yakhot–Orszag renormalization group method for deriving turbulence statistics and models. Phys. Fluids A: Fluid Dyn. (1989-1993) **4**(2), 364–390 (1992)
33. She, Z.S.: Intermittent vortex structures in homogeneous isotropic. Nature **344**, 15 (1990)
34. Batchelor, G.K.: The theory of homogeneous turbulence. Cambridge University Press, Cambridge (1953)
35. Ling, Y., Zaleski, S., Scardovelli, R.: Multiscale simulation of atomization with small droplets represented by a Lagrangian point-particle model. Int. J. Multiphase Flow **76**, 122–143 (2015)
36. Tryggvason, G., Scardovelli, R., Zaleski, S.: Direct numerical simulations of gas–liquid multiphase flows. Cambridge University Press, Cambridge (2011)
37. Klein, M., Sadiki, A., Janicka, J.: Investigation of the influence of the Reynolds number on a plane jet using direct numerical simulation. Int. J. Heat Fluid Flow **24**(6), 785–794 (2003)
38. Sander, W., Weigand, B.: Direct numerical simulation and analysis of instability enhancing parameters in liquid sheets at moderate reynolds numbers. Phys. Fluids (1994-present) **20**(5), 053,301 (2008)
39. Popinet, S.: An accurate adaptive solver for surface-tension-driven interfacial flows. J. Comput. Phys. **228**(16), 5838–5866 (2009)